Biogeosciences Discuss., 4, 823–869, 2007
www.biogeosciences-discuss.net/4/823/2007/

Biogeosciences Discussions

Biogeosciences Discussions is the access reviewed discussion forum of *Biogeosciences*

Iron profiles and speciation of the upper water column at the Bermuda Atlantic time-series Study site: a model based sensitivity study

L. Weber[1], C. Völker[2], A. Oschlies[3], and H. Burchard[4]

[1]National Oceanography Centre, Southampton, UK
[2]Alfred-Wegener-Institut für Polar- und Meeresforschung Bremerhaven, Germany
[3]Leibniz-Institut für Meereswissenschaften, Kiel, Germany
[4]Institut für Ostseeforschung Warnemünde, Germany

Received: 14 March 2007 – Accepted: 16 March 2007 – Published: 22 March 2007

Correspondence to: L. Weber (llw@noc.soton.ac.uk)

Abstract

A one-dimensional model of the biogeochemistry and speciation of iron is coupled with the General Ocean Turbulence Model (GOTM) and a NPZD-type ecosystem model. The model is able to simulate the temporal patterns and vertical profiles of dissolved iron (dFe) in the upper ocean at the Bermuda Atlantic Time-series Study site reasonably well. Subsurface model profiles strongly depend on the parameter values chosen for the loss processes for iron, colloidal aggregation and scavenging onto particles. Current estimates for these parameters result in depletion of dFe. A high stability constant of iron-binding organic ligands is required to reproduce the observed degree of organic complexation below the mixed layer. A solubility of atmospherically deposited iron higher than 2% lead to dFe concentrations incompatible with observations. Despite neglecting ultraviolet radiation, the model produces diurnal variations and mean vertical profiles of H_2O_2 and iron species that are in good agreement with observations.

1 Introduction

The recognition of the role of iron in limiting marine primary production has lead to attempts to measure the distribution and bioavailability of iron in the world's oceans (Johnson et al., 1997). Typically, total dissolved iron (defined as passing through a 0.2 μm or a 0.4 μm filter) is measured. A number of recent studies have enhanced our understanding of many of the processes that influence the speciation of iron, such as organic complexation (Gledhill and van den Berg, 1994; Van den Berg, 1995; Wu and Luther III, 1995; Rue and Bruland, 1995; Witter and Luther III, 1998; Witter et al., 2000), photochemical processes (Johnson et al., 1994; Emmenegger et al., 2001; Barbeau et al., 2003; Rijkenberg et al., 2004), redox reactions with peroxides (Voelker and Sulzberger, 1996) and interactions with colloids and particle surfaces (Johnson et al., 1994; Wen et al., 1997). However, there are still many unknowns in the complex iron

biochemistry in seawater due to the difficulty of direct measurement of chemical iron species in situ.

Numerical biogeochemical-physical models are now able to simulate the main patterns of total dissolved iron in the ocean (Dutkiewicz et al., 2005), but indicate that the details and in particular the climate sensitivity of so called "high nutrients low chlorophyll" (HNLC) regions, are strongly dependent of the way the iron chemistry is parameterised (Parekh et al., 2004). These models are typically forced by annual mean dust inputs (Mahowald et al., 2003) and have a simplified description of the marine iron chemistry that primarily aims at reproducing the scavenging removal of iron in the deep ocean and that is not adequate to simulate the response to the episodic nature of iron input by individual dust deposition events.

Modelling of iron cycling between its various species has recently been refined by Rose and Waite (2003) for coastal waters and by Weber et al. (2005) for the open ocean surface mixed layer. Rose and Waite (2003) focused on the chemistry of iron in short term experiments. In contrast, Weber et al. (2005) used a slightly less complex zero-dimensional model for iron chemistry coupled to an ecosystem model to study iron biogeochemistry in the mixed layer at the Bermuda Time-Series Station (BATS) Site. This model describes the cycling of iron between its various physical (dissolved, colloidal, particulate) and chemical (redox state and organic complexation) species and is influenced by atmospheric dust deposition, photochemistry, organic complexation, colloid formation and aggregation as well as uptake and release by marine biota. Weber et al. (2005) achieved results close to observed dissolved iron concentrations in the mixed layer. In contrast to the simple global speciation models, the model resolves processes with short time-scales, such as photochemical cycling and the rapid disappearance of iron after pulsed deposition events. However, the model contains some parameters, especially those for scavenging, colloid formation and aggregation that are not very well known. It was shown that these parameters have a strong influence on the vertical fluxes of iron, but, due to the limitations of a zero-dimensional model, did not affect the mixed-layer concentrations of dissolved Fe strongly. This means that

these parameters remained basically unconstrained.

In this study we describe an one-dimensional extension of the zero-dimensional model by Weber et al. (2005). In contrast to the zero-dimensional model, the one-dimensional approach allows an analysis of the depth dependency of the processes determining iron speciation and fluxes. Especially photochemical processes and biological activity can lead to vertical concentration gradients even within the surface mixed layer, which might influence the residence time and bioavailability of iron.

A couple of studies measured dissolved iron (dFe) profiles at the BATS site (Sedwick et al., 2005; Wu and Boyle, 2002; Wu et al., 2001; Wu and Boyle, 1998; Wu and Luther III, 1994), where dFe refers to 0.4 μm-filtered samples. Furthermore Wu et al. (2001) distinguished between soluble (0.02 μm-filtered samples) and colloidal iron (0.02–0.4 μm). Data reveal strong seasonal changes of dFe concentrations ([dFe]) in surface waters, with high concentrations in summer (up to 2 nM, Sedwick et al., 2005) and low concentrations in spring (down to 0.1 nM) (Wu and Boyle, 2002; Sedwick et al., 2005). The summer dissolved iron profiles of the different studies consistently show pronounced near surface maxima in [dFe], [dFe] minima in the 40–150 m depth range and increase in concentration between 150 m and 500 m to concentrations around 0.4–0.6 nM. The spring [dFe] profiles of the two studies have generally weaker gradients and lower concentrations of dFe than the summer profiles.

This study is aimed at a better general understanding of iron biogeochemistry and the role of iron speciation in it, an aspect so far neglected in most models. One outcome of this work is the identification of parameters that need to be better constrained in order to improve the prediction of speciation, concentration and fluxes of iron in the world ocean. The focus of this study is (i) the concentrations below the annual mixed layer and how they are affected by the parameterisation of loss processes that transfer dissolved iron to sinking particles either through scavenging or through a colloid intermediate; and (ii) the vertical scale of the fast redox cycling within the mixed layer. The model is primarily a tool to help in understanding the key processes of the iron cycle and their sensitivities to uncertainties in our present descriptions of these processes

rather than as a numerically accurate reproduction of reality.

This paper is organised as follows: after a description of the model in Sect. 2, results of the physical and ecosystem model components are described briefly in Sect. 3 and 4. In Sect. 5 we deal with the difficulty to reconcile slow iron loss processes at depth with short timescales in the mixed layer. In Sect. 6 we discuss the modeled diurnal and annual dynamics of the iron-cycle, followed by a study about the model sensitivity to parameter changes in Sect. 7 and 8. We conclude in Sect. 9, summarising the main outcomes of this study.

2 Model description

The model used in this study is a one-dimensional (1-D) extension of an earlier zero-dimensional (0D) model by Weber et al. (2005). It distinguishes between the following five iron species: dissolved inorganic ferric iron $Fe(III)'$ and ferrous iron $Fe(II)'$, organically complexed iron FeL, colloidal iron Fe_{col} and iron bound to the surface of sinking particles Fe_p. Furthermore the model calculates the concentrations of hydrogen peroxide ($[H_2O_2]$) and superoxide ($[O_2^-]$) as well as of sinking particles, both inorganic from dust deposition and organic from detritus. Most determinations of organic complexation of iron in seawater have shown an excess of truly dissolved organic ligands over total dissolved iron (e.g. Rue and Bruland, 1995; Van den Berg, 1995; Wu and Luther III, 1995; Witter and Luther III, 1998) but the sources of these ligands remain largely unknown. Therefore we assume a fixed concentration of free iron-binding organic ligands L, taken from the work by (Cullen et al., 2006) to ensure an excess of ligands. The processes converting iron between its different forms (see Fig. 3) are parameterised as in Weber et al. (2005), from which we adopted initial rate constants. The only exception is the photoreduction rate of colloidal iron (k_{ph1}). Estimates of k_{ph1} by Wells and Mayer (1991) and Barbeau and Moffett (1998) are much lower (between 0.12 and $0.43\,d^{-1}$) than the value by Johnson et al. (1994) ($20.16\,d^{-1}$), used by Weber et al. (2005). The latter value was calculated from data obtained by Waite and Morel (1984)

at pH 6.5. Johnson et al. (1994) assumed that this rate was the same at pH 8, which is not a reasonable assumption (King et al., 1993; Moffet, 2001). Daily values of dust deposition were taken from the output of a global atmospheric dust transport model by Mahowald et al. (1999).

The biological part of the model is the nitrogen-based ecosystem model by Oschlies and Schartau (2005) with four compartments, representing inorganic nitrogen (N), phytoplankton (P), zooplankton (Z) and detritus (D). Oschlies and Schartau (2005) calibrated the ecosystem model in a one-dimensional mode against observations at the Bermuda Atlantic Time-series Study site and two other sites in the North Atlantic (Table 1). In contrast to Weber et al. (2005), who assumed a uniform Fe:N ratio in phytoplankton, zooplankton and detritus, we allow for a decoupling between the cycling of Fe and N by reducing the uptake of iron under low concentrations of the Fe species taken up. This requires an explicit modelling of the Fe content in the ecosystem compartments, i.e. the addition of three further model equations (see Appendix). However, it is generally thought that phytoplankton is not iron-limited at the BATS site (Fung et al., 2000; Watson, 2001). Therefore we do not make the phytoplankton growth rate dependent on the iron quota of the cells or the external iron concentration. This assumption effectively makes nitrogen cycling independent from that of iron and helps to analyse the sensitivity of the iron cycle to parameter changes without feedback through changing export production. When applying the model to other oceanic regimes, iron limitation of phytoplankton growth should be taken into account.

The physical part of the model is the General Ocean Turbulence Model (GOTM: http://www.gotm.net and Burchard et al., 2006). We choose GOTM because it uses state-of-the-art turbulence closure models, which is a precondition for properly simulating vertical profiles of reactive biogeochemical quantities. For the present study, a two-equation k-ε model with an algebraic second moment closure by Cheng et al. (2002) was chosen (see Umlauf and Burchard, 2005 for the consistent implementation of this scheme). Furthermore, GOTM provides stiff equation solvers appropriate for dealing with the very fast photochemical reaction rates in the model (order of seconds).

In particular we used the recently developed non-negative and conservative modified Patankar-type solvers for ordinary differential equations (Burchard et al., 2005; Burgeman et al., 2006). Meteorological data are derived from the ERA-40 reanalysis project (Uppala et al., 2005) to drive the physical model. Sea surface temperature and salinity were restored towards observations with a time-scale of 5 days. We used the light extinction routine after Jerlov (1968); Paulson and Simpson (1977) provided by GOTM. Photosynthetically available radiation is assumed to be 43% of the total incoming irradiance (Brock, 1981). Ultraviolet radiation (UV) is not separately calculated although we are aware that it might also be important for the iron chemistry at the surface (Kuma et al., 1992; Rijkenberg et al., 2005). According to Jerlov (1968) and by adjusting the parameter for attenuation due to chlorophyll and water, we choose the oceanic type IB, which gave best model results for nutrient and chlorophyll alpha concentration, close to observations (Sect. 4).

A timestep of 1 min was chosen for the integration. It turned out that, together with GOTM's stiff equation solver, such a timestep is short enough to deal with the fast photochemical reaction rates. The short timesteps allow also to analyse the iron biogeochemistry over the course of a day. A total period of 9 years (covering the period from the beginning of 1988 until the end of 1997) was integrated, of which the first two years are spin-up time. The vertical grid consists of 100 layers over 600 m, with layer thickness increasing non-linearly from 0.9 m in the upper layer to 12.45 m at 600 m depth. All sinking biogenic matter is instantaneously remineralised in the lowermost model box. As we are considering here only the upper 250 m of the water column, this assumption does not affect model results within the timescale of the experiments.

3 Results of the physical model

The annual cycle of the physical properties in the model is driven primarily by seasonal changes in surface heat flux and wind stress. Strong thermal stratification is present in summer, largely due to higher heat fluxes and lower wind stresses. The modeled tem-

perature and salinity profiles as well as the mixed layer depth are in good agreement with observations (Steinberg et al., 2001): In summer, the mixed-layer has temperatures around 25°C, and is generally of reduced salinity. There is a subsurface salinity maximum, and strong density gradients in the upper 100 m. Temperature fluctuation of the surface layer (top 1–2 m), associated with the diurnal thermal cycle, ranges from 0.2 to 2.5°C depending on the net daytime surface heat flux (controlled by cloud cover and wind stress) and mixed-layer depth. In winter, the mixed layer is more saline and mean temperatures are around 19°C, while mixed-layer depths vary from 150 to 250 m. In summary, the GOTM results show a good fit to the observations and meet the requirements of the present study.

4 Results of the ecosystem model

The ecosystem model has already been used to study the nitrogen cycle at the BATS site with good results (Oschlies and Schartau, 2005). However, this study used a different physical model and different forcing fields. We therefore briefly present here the main features of the biological model solution.

The biological part of the model calculates dissolved inorganic nitrogen (DIN) and chlorophyll α (Chl α) concentrations, that are close to observations (Fig. 1).

DIN concentrations at the BATS site are low in the upper ocean (lower than 1 μM N), reflecting the oligotrophic conditions in the North Atlantic subtropical gyre. In late winter, the deepening of the mixed layer leads to a peak in DIN concentrations. The model reproduces this annual cycle quite well, with overestimation of DIN concentrations (by around 1 μM N) at the spring maximum. The modeled vertical DIN gradients are also close to those observed, with slight underestimations (by around 1 μM N) in seasonal variability of DIN below 120 m.

The distribution of Chl α at the BATS site is characterised by a spring bloom that is initiated by the increasing irradiance during the annual shoaling of the mixed layer, and later by the development of a deep chlorophyll maximum below the shallow summer

mixed layer. The modeled timing of the spring bloom is in good agreement with observations. During late spring and summer the modeled concentrations reveal a deep Chl α maximum similar to observations. Chl α concentrations are slightly overestimated in the model, especially in the upper 60 m (around 0.1 $\mu g\,l^{-1}$) Lower concentrations in Chl α were observed in years 1990–1991 which are not reproduced by the model.

The annually averaged vertical sinking flux of detritus at 100 m depth varies between 0.67 and 0.83 mol C m^{-2} a^{-1}. Taking into account also the vertical diffusion of particulate organic nitrogen ($PON=P+Z+D$) we get annually averaged vertical fluxes varying between 0.79 and 1.64 mol C m^{-2} a^{-1}. This is within the range of published estimates of export production at the BATS site (0.7 to 4.4 mol C m^{-2} a^{-1}, Carlson et al., 1994), albeit at the lower end. Both the assumption of a constant C:N ratio of 6.625 in organic matter and the lack of a dissolved organic carbon pool might cause the export production of the model to be biased somewhat downward.

The ecosystem model results show some deficiencies, such as an overestimation of summer concentrations of dissolved inorganic nitrogen and chlorophyll, which are, however, not uncommon for this type of ecosystem studies, especially without using data-assimilation methods. For the purpose of this study, however, it is mainly the modeled vertical export flux and the magnitude and timing of primary production, which are important. These quantities are in agreement with observations within the observational scatter. Model solutions for P_{Fe}, Z_{Fe} and D_{Fe}, i.e. the iron content in the ecosystem model, depend on the dissolved iron concentrations in the water column and will be discussed in the following sections.

5 Iron fluxes below the mixed layer

5.1 Initial state

For the initial model run of the present study (Run I), the same parameter set for the iron chemistry is used as in the zero-dimensional model of Weber et al. (2005) (Table 2;

apart from the photoreduction rate of colloidal iron as discussed above). This setting generates results far away from observations: Modeled iron concentrations within the mixed layer vary between 0.2 nM in summer and 1 pM in spring. Because of the very low [dFe] values in the mixed layer, uptake of iron by phytoplankton is strongly limited, leading to Fe:N quotas in the ecosystem model far below the maximum. Below the mixed layer, concentrations are lower than 1 pM. This result is independent of the chosen bottom boundary condition. In contrast, observations at the BATS site show annual variations between 0.1 nM and 2.0 nM at the surface, a subsurface minimum around 0.1 nM near 100 m depth, and values between 0.4–0.6 nM below (Wu and Boyle, 2002; Sedwick et al., 2005).

The main difference to the 0-dimensional model, where the same parameter set had produced results in accordance with observations (Weber et al., 2005), is that in the 1D approach the concentration of dissolved Fe below the surface mixed layer is generated by the model itself instead of being prescribed. This indicates that either the sources of iron at depth from remineralisation or physical transport are underestimated or that the modeled iron sinks from scavenging and aggregation at depth are overestimated in the current model setting.

The modeled physical transport of dissolved iron is unlikely to be a major model deficiency: Vertical diffusion is rather low in the model ($<1\,cm^2\,s^{-1}$), in agreement with observational estimates by Musgrave et al. (1988) and Ono et al. (2001). Lateral advection, which is neglected in a 1-dimensional model, could be a missing source of iron in the model. However, given the small current velocities (McClain and Firestone, 1993), this would require large horizontal dFe gradients at depth.

The main problem in this model setting occurs to be the loss of dissolved iron through formation and aggregation of colloids and scavenging. From observations of dissolved iron it has been estimated that the scavenging residence time of iron in the deep ocean is around 200 years (Johnson et al., 1997; Bergquist and Boyle, 2006). Close to the surface however, residence times for dissolved iron concentrations are estimated to be in the order of 1 to 5 months (Bergquist and Boyle, 2006). But even removal of

dissolved iron on timescales of days or less has been observed in iron fertilisation experiments (Nishioka et al., 2005). This loss operates through the association of dFe with suspended colloids by surface complexation and subsequent aggregation of these colloids with filterable particles. The one-dimensional model needs to reconcile slow iron loss losses at depth with fast removal in the mixed layer.

5.2 Reconciling slow iron loss processes at depth with short timescales in the mixed layer

The concentration of iron (in its different forms) below the mixed layer must adapt itself in the long-term average such that the source of dissolved iron, which is predominantly the remineralisation of organic matter, equals losses such as the transfer of dissolved forms of iron to to the particulate pool by scavenging and colloid aggregation. That this balance results in iron concentrations that are much lower than observations can have three explanations: (i) the assumed rates for colloidal aggregation and/or scavenging are too large and/or (ii) organic complexation processes, which increase the residence time of iron, are too weak and/or (iii) the modeled sources of iron are too small.

Point (iii) will be discussed in Sect. 8. A qualitative understanding of (i) and (ii) can be obtained from a simplified calculation: If we neglect photochemistry, vertical transport and temporal variability, we obtain the following three balances for dissolved iron species:

- colloid formation equals aggregation loss,

$$0 = k_c \mathrm{Fe(III)}' - k_a \mathrm{Fe_{col}} \quad (1)$$

  where $k_a = k_{ag}(P + r_{m:N} D)$ is the effective aggregation rate

- dissociation equals formation of organic iron complexes – scavenging – colloid formation

$$0 = k_{ld} \mathrm{FeL} - k_{\mathrm{fel}} \mathrm{Fe(III)}' L - k_s \mathrm{Fe(III)}' - k_c \mathrm{Fe(III)}' \quad (2)$$

where $k_s = k_{sca}(P + r_{m:N}D)$ is the effective scavenging rate

– remineralisation of iron from decay of organic matter + complex formation equals complex dissociation,

$$0 = R + k_{fel}\mathrm{Fe(III)}'L - k_{ld}\mathrm{FeL} \quad (3)$$

where R is the iron remineralisation rate $R = r_{Fe:N}\gamma_d D$

From these balances we obtain

$$\mathrm{Fe(III)}' = \frac{R}{k_c + k_s} \quad (4)$$

$$\mathrm{Fe_{col}} = \frac{k_c}{k_a}\frac{R}{k_c + k_s} \quad (5)$$

$$\mathrm{FeL} = \frac{R + k_{fel}\mathrm{Fe(III)}'L}{k_{ld}} \quad (6)$$

Average modeled values of detritus and inorganic particle concentrations at 250 m depth are D=0.0086 μM and P=1.3 mg l^{-1}. At these concentrations of particles, k_s is much lower than k_c. To first order $\mathrm{Fe_{col}}=R/k_a$ and $\mathrm{Fe(III)}'=R/k_c$, i.e. the colloidal iron concentration is inversely proportional to the colloid aggregation rate, and the inorganic iron concentration is inversely proportional to the colloid formation rate. Calculating R from the models temperature and detritus concentration and by inserting the parameter values of the iron model of Weber et al. (2005), we obtain $\mathrm{Fe_{col}}$=0.3 pM and FeL=0.9 pM. These values are orders of magnitude lower than observed ones. From Eq. (5) it is obvious that the only way to bring $\mathrm{Fe_{col}}$ into better agreement with observations is to decrease the colloid aggregation rate k_{ag}. FeL can be increased by either increasing the ligand strength (i.e. decreasing k_{ld}) or by increasing $\mathrm{Fe(III)}'$ through decreasing k_c, or by a combination of both.

Under the assumption that k_c has already the correct order of magnitude (see Sect. 5.3.1), an increase of k_{ld} by a factor of 50 as well as a decrease of k_{ag} by a factor of 1000 yields Fe_{col} = 0.3 nM and FeL = 0.1 nM.

These qualitative considerations results in parameters modified (Run A) accordingly to k_{ag}=1224 and k_{ld}=10^{22} (see Table 2). Results of the 1-D-model with this set of parameters are close to observations and will be discussed in more detail in Sect. 6.

Run A will be referred as the standard model run of the present study.

5.3 Is the parameter modification justified in terms of observations?

5.3.1 Colloidal aggregation

The colloidal aggregation rate needs to be three orders of magnitude lower than in the zero-dimensional model to achieve model results close to observations. In spite of low particle concentrations in the open ocean it is suggested that marine colloids are very dynamic with high colloidal aggregation rates (Moran and Buesseler, 1992; Baskaran et al., 1992). So far, there are no methods to measure colloids directly in situ in seawater at typical oceanic concentrations. Detailed processes that lead to changes in particle size are not fully understood (Wells, 2002). This makes it difficult to represent colloidal processes in a model adequately. Wen et al. (1997) performed some radiotracer experiments to study the interactions between ionic, colloidal and natural particulate forms of iron. From this work, Weber et al. (2005) derived a colloidal aggregation rate, proportional to the concentration of particles and colloids. However, Wen et al. (1997) preformed the experiments with particle-rich waters (10 mg/L) from the Galveston Bay, at the coastline of Texas, USA. For the particle poor region at the BATS site (around 0.01 mg/L), conditions which lead to aggregation are different. The rate constant for the formation of colloidal iron, k_c, appears to be somewhat better constrained, e.g. by Johnson et al. (1994) who determined k_c by measuring the change in dissolved Fe(III) concentrations during dark periods from an initial concentration of 10 nM Fe(III).

5.3.2 Strong ligands

Weber et al. (2005) used a conditional stability constant of Fe-organic complexes of $10^{20.3}M^{-1}$, as was measured by Wu and Luther III (1995). However, the range of the measured conditional stability constants by different authors is wide and reaches from $10^{18}M^{-1}$ to $10^{22.5}M^{-1}$ (e.g. Gledhill and van den Berg, 1994; Wu and Luther III, 1995; Van den Berg, 1995; Cullen et al., 2006). Therefore, a large window of opportunity exists for the choice of the model's conditional stability constant, bearing in mind that in the ocean different classes of ligands with different binding strength exist (Gledhill and van den Berg, 1994; Cullen et al., 2006) and that the relatively simple representation made by the present model approach only allows for one "typical" class. The value $10^{22}M^{-1}$ that we use is within this admittedly large range of variation and agrees with the observed value for iron binding ligands in the Sargasso Sea by Cullen et al. (2006). However, different from Gledhill and van den Berg (1994) who found strong binding ligands throughout the water column, Cullen et al. (2006) suggested that in surface waters in the Sargasso Sea, strong ligands with a conditional stability constant of $10^{22.01}$ relative to total inorganic Fe appeared to dominate while in deep water ligands have stability constant 12–15 times smaller. The model cannot confirm these observations, since stronger ligands with a stability constant of around 10^{22} are required, especially below the mixed layer, to reproduce a decent iron profile. We realize that further model development in terms of different ligand classes is required. Since this will add new parameters to the model, such an approach will also need further information (qualitatively and quantitatively) from laboratory and field experiments with regard to the origin, strength and fate of organic ligands for iron in the seawater.

6 Temporal dynamics in the mixed layer

6.1 Diurnal variability of iron speciation

The modeled iron and reactive oxygen speciation shows a strong diurnal variablity in the upper water column (Fig. 2), similar to the results of the zero-dimensional model by Weber et al. (2005).

The modeled hydrogen peroxide (H_2O_2) concentrations follow a distinct diurnal pattern, with highest values during mid to late afternoon and lowest concentrations in the morning. The depth limit of diurnal variations in H_2O_2 concentration is variable, ranging from 20 m in winter to around 40 m in summer. The mixed-layer averaged concentration of hydrogen peroxide in the model demonstrates a strong annual cycle, varying between 25 nM in winter and around 65 nM in summer. These results are in good agreement with observations in the subtropical Atlantic by Obernosterer et al. (2001). They detected H_2O_2 concentrations of, on average, 42 nM in both surface waters and in profiles up to 50 m depth. This followed a distinct diurnal pattern with highest concentrations during mid to late afternoon and lowest concentrations during the morning. The lifetime of superoxide is extremely short (order of seconds) so that its modeled concentration correlates strongly to irradiance with maximum concentration at noon and zero values at nighttime. FeL and Fe_{col} are the dominant forms of iron during the night. During daytime the concentrations of $Fe(II)'$, $Fe(III)'$ become significant due to photochemical reactions. At the surface $Fe(II)'$ is produced by direct photoreduction of ferric iron species but mainly by the reduction of $Fe(III)'$ by photoreduced superoxide (Table 3). Consistent with the rates estimated by Voelker and Sedlak (1995), iron reduction by superoxide occurs at a rate that is up to more than a hundred times the maximum rate of all direct photoreductive processes taken together. Photoproduction of superoxide and its subsequent transformation to hydrogen peroxide leads to a corresponding cycle of iron redox-reactions and to an increase in $[Fe(II)']$ and $[Fe(III)']$ in the daytime at the expense of [FeL]. Variation in [FeL] between day and night is up to 60% at the surface. The $Fe(II)'$ produced is subsequently oxidised again to $Fe(III)'$ by O_2,

O_2^- and H_2O_2. Until midday, iron reduction outweighs oxidation, leading to an increase of $[Fe(II)']$, but also of $[Fe(III)']$ at the expense of [FeL]. In the afternoon, the balance between reduction and oxidation is reversed because $[H_2O_2]$ reaches its maximum, and $[Fe(II)']$ decreases. During the night all photochemical reactions stop so that all Fe(II)′ is oxidised to Fe(III)′, some of which is rapidly complexed by free organic ligands. The formation and photoreduction of colloidal iron in the model is a much slower process (one to two order of magnitudes) compared to organic complexation, oxidation and photoreduction (Fig. 3). Variations in $[Fe_{col}]$ between day and night are therefore in the order of a few percent (around 1% at the surface).

Light the driving force behind photochemical cycling decays strongly with depth. Compared to the surface, modeled photoreduction and oxidation rates are about one order of magnitude lower at 40 m depth and about four orders of magnitude lower at 100 m depth (Table 3). On the other hand, the strong vertical mixing within the mixed layer acts to oppose the creation of concentration gradients within the mixed layer. The vertical distribution of (directly or indirectly) photoproduced species, such as Fe(II)′ therefore depends on the equilibrium between mixing and production which is strongly affected by the life-time of the species. The shorter the life-time of a species is, compared to the time-scale of vertical mixing, the stronger its vertical distribution is coupled to that of its production (Doney et al., 1995). Model results clearly show strong vertical gradients in the amplitude of the diurnal cycle of all photoproduced species (superoxide, Fe(II)′, Fe(III)′ and hydrogen peroxide) within the mixed layer. The different life-times of the different photochemically produced species are reflected in different depth depencedependencies their daily cycle (Fig. 4).

The concentration of the shortest-lived species, superoxide, decreases strongest with depth, while the daily cycle of hydrogen peroxide is less directly related to the exponential decrease of light intensity. The creation of vertical gradients within the mixed layer is enhanced by the stastabilisation the water column during the day by solar warming. The redox-reactions of inorganic Fe and organic complexation determine the residence time of dissolved iron in the euphotic zone by keeping iron in solution (Fe(II)′,

Fe(III)′ and FeL) and therefore preventing it from scavenging or building colloids and subsequently aggregating. Therefore, a distinct profile of [dFe] develops with higher concentrations of iron at the surface, strongly decreasing then over the upper 40 m with decreasing light availability. Additional to the decrease in photochemical activity with depth, a [dFe] minimum develops between 40 and 100 m due to increased biological activity at this depth (Sect. 4). Below the deep chlorophyll maximum [dFe] increases back to a concentration of appapproximately 6 nM due to remremineralisation organic detritus.

The model results agree well in summer with observations by Wu and Luther III (1994) (Fig. 5). A similar vertical pattern is also observed by Sedwick et al. (2005) but with a greater range between maximum and minimum concentrations of the profile. The iron profile concentrations in spring ar simular to the observations by Wu and Boyle (1998), with smaller differences between minimum and maximum concentrations in spring than in summer.

6.2 Annual cycle and interannual variability of dissolved iron

The modeled concentration of dissolved iron in the mixed layer ranges from 0.56 nM in spring to 0.85 nM in summer (Fig. 6, bottom), which is a little higher than observations by Wu and Boyle (2002) (0.2–0.6 nM) and within the range of observations by Sedwick et al. (2005) (0.1–2 nM). These iron concentrations are never limiting for phytoplankton uptake. Therefore the Fe:N quota in phytoplankton, zooplankton and detritus are always close to the prescribed maximum quota $r_{Fe:N}$, justifying a posteriori our neglection of iron limitation for phytoplankton growth. The model seems to overestimate the minimum [dFe] concentrations, possible because of the low value required for colloidal aggregation in the present model (see also Sect. 8).

The range of iron concentration over the year is subject to a strong seasonal cycle of [dFe], caused by the annual mixed layer cycle, spring phytoplankton bloom and dust deposition.

Winter deepening of the mixed layer leads to dilution of [dFe]. Increased detritus

concentrations in March and April, caused by the spring phytoplankton bloom, support colloidal aggregation and scavenging, which lead to a further drawdown in [dFe]. Additionally, the uptake of iron by phytoplankton is increased at this time. The main import of iron occurs in summer when dust storms from the Sahara arrive. At this time the mixed layer is shallow and phytoplankton activity is low. The import of atmospheric iron increases [dFe] in the surface water until the winter deepening of the mixed layer starts again.

The annual cycle of modeled Fe contains no significant interannual variability in dFe concentration and speciation. In contrast to that, the dust deposition has a intinterannualriability, with changes by a factor of more than 2.5. Changes in iron input due to increased dust deposition are buffered by a change in the residence time of dFe (Sect. 6.3) due to associated increase in particle concentration and therefore increased colloidal aggregation and scavenging.

6.3 Residence time of iron

The residence time of dissolved iron is usually defined as the ratio between the total dissolved iron concentration (in nmol/l) and the rate at which dissolved iron is lost (in nmol/l/d). Typically, a constant scavenging residence time, i.e. a proportionality between dissolved iron concentration and scavenging loss is assumed. However, iron speciation, and nonlinearities in the dependency of loss on concentrations may make this assumption invalid. In the present model these processes are at least partially resolved. It is therefore interesting to investigate how the effective residence time in the model varies over time and depth, as we had to change the colloid aggregation rate in such a way that the model results are consistent with subsurface observations (Sect. 5.2).

We concentrate here on the residence time with respect to scavenging and colloid aggregation, i.e. the two processes that transfer iron from the colloidal and dissolved

phase to filterable particles. This rate is formally defined by

$$\tau = \frac{[\mathrm{Fe(III)}'] + [\mathrm{Fe(II)}'] + [\mathrm{Fe_{col}}] + [\mathrm{FeL}]}{\left(k_{ag}[\mathrm{Fe_{col}}] + k_{\mathrm{sca}}[\mathrm{Fe(III)}']\right)\left([A] + [D_{\mathrm{Fe}}]\right)} \quad (7)$$

where $[A]$ is the concentration of inorganic particles.

The annual cycle of τ at the surface shows values up to 30000 days in winter when neither organic nor inorganic particles are present in great numbers. This is of the same order of magnitude as estimates for the deep ocean (see Sect. 5.1). The residence time is reduced markedly to approximately one hour in late spring following the phytoplankton spring bloom.

The phytoplankton bloom influences the residence time negatively by uptake of dFe directly but also indirectly by producing detritus. A second reduction in the residence time occurs in summer as a consequence of dust deposition events (Fig. 7). In winter, the smaller deposition of atmospheric iron remains within the mixed layer longer, while in summer the higher deposition leads to a stronger source, but also to a faster loss because of the increased particle density.

7 Parameter sensitivity

As for all numerical models, the particular solution depends on the choice of biogeochemical parameters. Some of the model parparameterisations.g. for colloid aggregation, attempt to describe a complex process in a simple way. Estimation of the corresponding parameters therefore remains a major challenge. Even though some of the parameters of this study are based upon measurements taken in the laboratory and the ocean, most are based on approximations and also often on pragmatic assumptions. It is therefore necessary to investigate the sensitivity of the model results to changes in the parameter values that are most uncertain.

Because of the large number of parameters involved, we limit the sensitivity tests to variations in one parameter at a time, leaving all other parameters unchanged (Table 2,

Run A). We conducted two sensitivity runs per parameter, one with a 50% lower and one with a 100% higher value. For purposes of comcomparisone did the same with the zero-dimensional model. The main effects of these parameter changes on dissolved iron concentrations are sumsummarised in Table 4.

7.1 Comparison of parameter sensitivity between 0-D and 1-D

Comparing the one-dimensional model results of the sensitivity study with model results of the same sensitivity study using the zero-dimensional model by Weber et al. (2005) (Table 4) reveals that the one-dimensional model is much more sensitive to parameter changes of the main sources and sinks (solubility of atmospheric iron, colloidal aggregation and uptake by phytoplankton).

Model results of the zero-dimensional model indicate an important role of the vertical flux of iron due to the entrainment and detrainment of water during the annual cycle of mixed layer deepening and shoaling (Weber et al., 2005). This flux is dominant in the sense that it balances the other fluxes in such a way that the total dissolved iron concentration in the mixed layer does not depend strongly on the size of dust input, colloidal aggregation or uptake (Table 4), but remains tightly coupled to the concentration below the mixed layer, which is prescribed. In the one-dimensional model, iron profiles below the mixed layer have to be generated by the model itself (see also Sect. 5.1). This leads to bidirectional feedbacks. Changes in the surface fluxes are not necessarily compensated by the exchange with deeper water anymore and need to be balanced in other ways. However, the vertical exchange in the one-dimensional model can buffer the sensitivity of certain fluxes as well. The most distinct example of this is the solubility of atmospheric iron. One would expect that doubling k_{sol} would increase [dFe] in the mixed layer by more than only 13%, bearing in mind that dust deposition is the main source of iron in the model. Here, the higher solubility of iron is buffered by changes in vertical iron fluxes in the same way than the interannual variability of dust deposition hardly influences the interannual consistency of dFe (see Sect. 6.2). The one-dimensional model confirms therefore the results by Weber et al. (2005), that the

concentration of dFe in the mixed layer is strongly regulated by the concentration below the mixed layer.

7.2 Atmospheric iron

Estimates of the solubility of iron from dust vary between 0.1% and 50%, (Zhuang et al., 1990; Duce and Tindale, 1991; Spokes and Jickells, 1996; Jickells and Spokes, 2001; Baker et al., 2006).

Changing the solubility of dust-deposited iron (k_{sol}) in the model has the strongest effect on [dFe] in surface waters of all parameters. In contrast to that, changes due to changes in k_{sol} are rather small at depth.

The main deposition of atmospheric iron occurs in summer when the mixed layer is shallow and the mixed layer prevents exchange with deeper water. A higher solubility leads therefore to a higher accumulation of iron in the upper water column. The solubility of atmospheric iron influences the annual mean profile of [dFe] down to 200 m with the strongest effect at the surface and a decreasing effect with depth. Almost all atmospheric iron which dissolves forms FeL, since the formation of organic complexes is a faster process than the formation of colloids (see Sect. 6.1). Hence an increase in solubility leads to an increase in [FeL] and the additional iron is kept in solution. Winter mixing brings it down to 200 m.

Increasing the solubility leads to an increase in both maximum and minimum dFe concentrations at the surface. As the spring minimum in dissolved iron is already quite high compared to observations, a solubility higher than about 2% seems unlikely.

7.3 Iron uptake

Changes in the maximum Fe:N-ratio in phytoplankton ($r_{Fe:N}$) affect the uptake of iron by phytoplankton and the amount of iron released during remremineralisation detritus. At the parameter values used (Table 2, Run A) iron is never limiting to phytoplankton so that the actual Fe:N ratio in phytoplankton, zooplankton and detritus is always close

to the maximum.

An increased uptake due to doubling of $r_{Fe:N}$, decreases the mean concentration of dFe in the surface by 6% on average. During the phytoplankton bloom in spring [dFe] can be up to 9% lower. The increased uptake on the other hand leads to an increase in deep dissolved iron concentrations. The changes are strongest near the depth of maximum remremineralisationear 100 m depth), but at 250 m depth the increase in dFe concentration is still 2%.

This leads to a profile of [dFe] with a more pronounced difference between minimum concentrations at 50 m depth in the annual average and a local maximum below. Consequently, a smaller value of $r_{Fe:N}$ leads to less uptake, less remremineralisationd a more uniform dFe profile with less difference between minimum and maximum concentrations. A profile like the one with higher $r_{Fe:N}$ comes closer to observed profile characteristics (Sect. 6.1). Sedwick et al. (2005) observed even higher differences between minimum and maximum concentrations, both more extreme. Hence, the model results reflect a higher maximum Fe:N-ratio than initially allowed. Bergquist and Boyle (2006) estimate an Fe:C ratio for the North Atlantic which is appapproximatelyice the Fe:C-ratio which Weber et al. (2005) used for their model to calculate the Fe:N-ratio. The North Atlantic may have elevated Fe:C ratios compared with most of the ocean owing to the higher surface dFe and luxury Fe uptake by organisms (Sunda and Huntsman, 1995).

7.4 Colloids and ligands

The parameters relating to organic complexes and colloids were discussed already in Sect. 5.2. One has to bear in mind that the uncertainty in the rates of colloidal aggregation and in the strength of organic complexes is orders of magnitude higher than the 50% to 100% range used in the sensitivity experiments here, for consistency, for all parameters.

Changes in the colloidal aggregation rate k_{ag} have the largest effect, as they change the concentration of dFe almost uniformly throughout the profile with a slightly greater

effect below the mixed layer. Doubling the value of k_{ag} leads to a 5% decrease of [dFe] in the upper 100 m and a 7% decrease below the mixed layer (250 m). The effect is stronger in deeper water because the photochemistry, which leads to redissolution of colloids in surface waters, vanishes with depth (see Sect. 6.1). In our sensitivity experiments, the effect of changes in colloid formation, the scavenging rate or the strength of ligands on [dFe] is much smaller (maximal 2%) than that of changes in k_{ag}. However, the speciation of iron is affected in different ways: Changing the colloid formation rate k_{col} leads to a shift between $\mathrm{Fe}_{\mathrm{col}}$ and FeL throughout the whole profile, where, e.g. doubling the value of k_{col} leads to higher $\mathrm{Fe}_{\mathrm{col}}$ concentration (around 0.08 nM) and consequently to higher export fluxes through colloidal aggregation (approximately 88% higher).

Changing the ligand formation rate k_{fel} leads to a shift between [$\mathrm{Fe}_{\mathrm{col}}$] and [FeL] (around 0.05 nM), but mainly in the upper 200 m, where higher k_{fel} leads to higher [FeL] at the expense of [$\mathrm{Fe}_{\mathrm{col}}$]. The model is more sensitive to this value in the upper water column due to higher production of inorganic redox forms by photochemical processes at the expense of both [$\mathrm{Fe}_{\mathrm{col}}$] and [FeL] during the day, but mainly subsequently through complexation by free organic ligands in the nightime (see Sect. 6.1). This effect decreases with depth but reaches as far as 200 m because of the deep winter mixing. In contrast, changing the ligand stability k_{ld} leads to a shift between $\mathrm{Fe}_{\mathrm{col}}$ and FeL only below the photic zone. A higher value of k_{ld} leads to higher $\mathrm{Fe}_{\mathrm{col}}$ concentrations at the expense of [FeL] (up to around 0.08 nM). Below 50 m, photochemical processes do not support organic complexation anymore.

Overall, the impact of changes of the parameters k_{col}, k_{fel} and k_{ld} is small compared to that of changes in other parameters. A more detailed discussion of these processes has to await a significant reduction in the still substantial conceptual uncertainties, such as the paparameterisationf colloidal aggregation.

7.5 Photochemical processes

Model results (Table 4) suggest that iron chemistry below the mixed layer is relatively insensitive to most parameter changes of this order of magnitude. This is especially true for all photochemically influenced processes since these have no immediate impact at this depth. However, even in the upper 100 m, oxidations processes are also insensitive to their parameter changes. While these processes are important in controlling iron speciation and concentration in the upper water column (Sect. 6.1), their relatively insensitivity to dFe concentration arises through the fast photochemical reactions ococcurringuring the day, making these two species important "reloading points". Reducing these rates by 50% slows down the cycle between Fe(III) and Fe(II)′ but does not take away the dominance of these processes, which are still up to two orders of magnitude faster than all other processes of the iron cycle during the day.

In contrast to the insensitivity to photoreduction of Fe(III)′ and Fe_{part} (k_{ph3} and k_{ph4}), the small (1%) but finite sensitivity due to doubling or halving the photoreduction rates of Fe_{col} and FeL (k_{ph1} and k_{ph_2}) is due to the difference in the respective iron concentrations. Fe_{col} and FeL are the dominant forms of iron in the mixed layer. Hence, doubling or halving their photoreduction rates has a greater impact.

The concentration difference of dFe is caused by a shift in the speciation of iron by changing k_{ph1} or k_{ph_2}. Doubling k_{ph1} leads to an increase of [FeL] at the expense of [Fe_{col}] and vice versa. This allows iron to remain in solution longer by increasing FeL, or increasing Fe_{col} allowing higher export fluxes due to increased colloidal aggregation by increased Fe_{col}. This effect reaches down to 200 m, where the concentration of the species eqequaliseith the concentrations from the standard model run.

This is especially interesting for k_{ph1}, since the importance of photoreduction has been revealed in field studies using ferrihydrite as a model solid but there is a lack of data on naturally occurring colloids (Moffet, 2001). There is a need to quantify these parameters through laboratory and field studies to validate the model.

The model still has a relatively simplistic representation of photochemical reactions

which are assumed to vary with irradiance over the visible band.

Recent deck-incubation experiments with open ocean water showed, that the UV part of the solar spectrum plays a major role in the photoreduction of iron, suggesting that any increases in UV (e.g. stratospheric ozone depletion) could increase the formation of Fe(II) and therefore the residence time and bioavailability of iron in the euphotic zone (Rijkenberg et al., 2005). However, in seawater UV is much more attenuated with depth than the visible band. In momoderately productive water UV-B does not reach 10 m depth whereas visible light penetrates down to 50 m (Smith and Baker, 1979). Taking into consideration that doubling the photoreduction rates hardly influences the dFe concentration, an explicit consideration of UV in the model is of less relevance to the total iron concentration than to the speciation of iron in the upper water column.

8 Introducing redissolution of particulate and colloidal iron

The low colloid aggregation rate required to reproduce observed iron concentrations (Sect. 5.2) has a strong influence on the temporal behaviour of iron concentrations within the mixed layer. In particular, the model now lacks the observed rapid decrease of [dFe] after pulsed iron additions (Nishioka et al., 2005).

The reduction in the aggregation rate is a consequence of the model setup in which there is no way back from particulate and/or colloidal iron to truly dissolved forms, other than photochemistry, which vanishes completely in the deep ocean.

One could therefore argue that an alternative to reducing the aggregation rate could be to introduce leaching of particulate iron and/or colloidal iron back into dissolved form, as in Parekh et al. (2004). Desorption of iron bound to particle surfaces as well as dissagregation processes and break-up of colloids are not unlikely but the processes driving them and their rates are still not very well understood (Moffet, 2001).

To investigate the effect of redissolution on deep iron concentrations we add two additional source terms of iron in the equation for $Fe(III)'$ and the corresponding sinks in the equation for particulate iron (Fe_p) and colloidal iron (Fe_{col}). The processes are

parameterised as linearly dependent on the concentrations as,

$$\psi_p = k_{pd}[\mathrm{Fe}_p] \quad (8)$$

$$\psi_c = k_{cd}[\mathrm{Fe}_{\mathrm{col}}] \quad (9)$$

with ψ_p indicating the flux from Fe_p to Fe(III)′ and ψ_c the flux from $\mathrm{Fe}_{\mathrm{col}}$ to Fe(III)′.

In the absence of information regarding rates for these processes, we choose rates that are of the same order of magnitude as photochemical dissolution rates in the mixed layer, $k_{pd} = k_{cd} = 0.2\ d^{-1}$. Both are probably at the very upper end of possible rates, and are also significantly higher than estimates by Parekh et al. (2004) (20–100 y^{-1}). However, the slow redissolution rate in Parekh et al. (2004) complements an equally slow scavenging rate, while we also attempt to represent faster processes.

We performed three additional experiments with redissolution, one including ψ_p (Run r1), one with ψ_c (Run r2), and one with both processes (Run r3). For these experiments the initial colloidal aggregation rate by Weber et al. (2005) is used, while the conditional stability constant of iron binding ligands is taken from the present study (Run A). This allows comparison of the results of this experiment with results from Run A.

A summary of [dFe] in these experiments is shown in Table 5. In all experiments, dissolved iron concentrations are increased with respect to the case of the initial model run (Run I).

Results of the model runs with either ψ_p (Run r1) or ψ_c (Run r2) show that introducing these relatively high rates does not solve the problem entirely and that the high aggregation rate of colloidal iron leads to iron depletion at depth. However, the concentration of dFe below the mixed layer is around 50 pM in Run r1 and 1 pM in Run r2, which is up to more than two order of magnitude higher than in Run I (Table 5). The concentration in the mixed layer is likewise three times higher than in the initial model run. The maximum concentrations in the mixed layer are of the same order of magnitude to observations by Wu et al. (2001) and Sedwick et al. (2005). The minimum concentrations are one order of magnitude lower than observations. The annual minimum of [dFe] in the mixed layer remains relatively low, even in the run with k_{pd} and

k_{cd} together (Run r3). The same holds for the concentration of dFe below the mixed layer, although it is interesting to note that the increase in [dFe] with respect to Run I is larger than the sum of the increases in Runs r1 and r2.

Compared to the standard model run (Run A) with reduced colloidal aggregation rate, the amplitude of the annual cycle of [dFe] (difference between maximum and minimum value in Table 5) in the mixed layer is increased in all of these experiments. The annual pattern, with a minimum in early spring and a maximum in summer remains the same.

In summary, the model runs in this Section show that redissolution can lead to deep water and mixed layer concentrations of dFe that are closer to observed values, even with high colloid aggregation rates. However, the resulting [dFe] remains systematically too low even for probably unrealistically high redissolution rates. This further confirms that the colloid aggregation rate has to be lower than the value used by Weber et al. (2005). It is probable that by varying the colloid aggregation and redissolution rates simultaneously over the range of values considered here, a solution can be found that reproduces both the observed deep iron concentrations and the rapid removal of iron from the dissolved phase in iron fertilisation experiments. However, such a systematic parameter study is outside the scope of the present paper. Introducing k_{pd} and/or k_{cd} might be especially interesting for future model studies with pulsed events, such as iron fertilisation experiments. However, such an improvement of the model will need further input from laboratory and field experiments with regards to the processes and rates in which redissolution of colloids and inorganic particles take place.

9 Conclusions

A one-dimensional model approach of an earlier model by Weber et al. (2005) was set up. We have demonstrated that the model, using parameter values guided by laboratory and field studies, is able to simulate the temporal patterns and the vertical profile of dissolved iron in the upper ocean for the Bermuda Atlantic Time series Study site reasonably well. However, the model solution still strongly depends on the choice

of some biogeochemical parameters. The main outcome of this study is as follows:

1. High colloidal aggregation rates of iron, observed in particle-rich coastal waters (Wen et al., 1997) and during iron fertilisation experiments (Nishioka et al., 2005) can not be applied to reproduce iron profiles at the BATS site with the current model. To prevent unrealistic depletion of dissolved iron at depth, the model requires aggregation rates 3 orders of magnitude lower than those observed, even when scaled with the concentration of sinking particles. Introducing a hypothetical redissolution of colloids or of iron bound to sinking particle surfaces also leads to less depletion of dissolved iron at depth in the model, but not enough to overcome the need to reduce aggregation rates.

2. A relatively strong iron binding ligand is required in the model, especially at depth, to prevent dissolved iron from aggregation and scavenging and to maintain a realistic iron profile. The required value for the conditional stability constant depends on the rate chosen for colloidal formation and is at the higher end of observed values.

3. The solubility of atmospherically deposited iron has a strong influence on the surface dFe concentration, especially in summer. Solubilities of more than 2% lead to modeled dFe concentrations that are higher than observations.

4. The Fe:N ratio in phytoplankton that corresponds to the "typical" Fe:C ratio of 5×10^{-6} (Sunda and Huntsman, 1995) leads to spring dissolved iron concentrations that are somewhat higher than observations, and to a not very pronounced vertical structure in the profiles with a weak minimum directly under the summer mixed layer and a maximum around 100 m depth. The agreement with observations by (Sedwick et al., 2005) is improved in those two respects when the Fe:N ratio is increased.

5. In the upper water column, the dominant processes affecting iron speciation are the photochemically driven redox-reactions of inorganic Fe and organic complex-

ation. These manifest themselves as a strong daily cycle of iron and reactive oxygen speciation in the mixed layer. These processes act on such short timescales that vertical gradients within the mixed layer are produced that are strongest for the very short-lived species such as superoxide and ferrous iron and somewhat weaker for longer-lived species, such as hydrogen peroxide. Both determine the residence time of dissolved iron in the euphotic zone by keeping iron in solution and therefore preventing it from scavenging. This is manifested as a dissolved iron profile with higher concentration at the surface and a strong decrease in the upper 50 m following the decreasing light availability.

The conclusions are based on a still very limited data set. Further measurements, especially time series of dissolved iron and its speciation, would be extremely helpful to validate the model. The sensitivity of the model to slight changes in the parametrisation of still unclear processes indicates that we are far away from understanding the influence of iron in the marine ecosystem and to predict it with confidence in global climate models.

Appendix

In addition to the chemical iron model by Weber et al. (2005) and the optimised NPZD ecosystem model by Oschlies and Schartau (2005) we implemented three further biological model equations that determine the evolution of the concentration of iron in phytoplankton P_{Fe}, detritus D_{Fe}, and zooplankton Z_{Fe}. The equations are based on the NPZD model by Oschlies and Schartau (2005) and are formulated in units of nM iron d^{-1}.

$$\frac{d}{dt}[P_{\mathrm{Fe}}] = r_{\mathrm{fe:p}}\rho[P] - r_{\mathrm{fe:p}}G([P])[Z] - \gamma_p(T)[P_{\mathrm{Fe}}] - r_{\mathrm{fe:p}}\gamma_{p^2}[P]^2 \quad \text{(A1)}$$

$$\frac{d}{dt}[Z_{Fe}] = r_{fe:p}\gamma_{za}G([P])[Z] - \gamma_{zb}(T)[Z_{Fe}] - r_{fe:z}\gamma_{z^2}[Z]^2 \quad \text{(A2)}$$

$$\frac{d}{dt}[D_{Fe}] = r_{fe:p}\gamma_{p^2}[P]^2 + r_{fe:p}(1-\gamma_{za})G([P])[Z] + r_{fe:z}\gamma_{z^2}[Z]^2 - \gamma_d(T)[D_{Fe}] - w_s\frac{d[D_{Fe}]}{dz} \quad \text{(A3)}$$

with $r_{fe:p} = [P_{Fe}]/[P]$ and $r_{fe:z} = [Z_{Fe}]/[Z]$.

The terms on the right hand side are identical to the terms in the NPZD model except for a multiplication with either $r_{fe:p}$ or $r_{fe:z}$. One exception is the uptake of iron by phytoplankton: While the growth rate of phytoplankton μ is the smaller of either a nutrient- or a light-limited rate $\mu = \min(\mu_N, \mu_L)$, the iron uptake rate ρ also depends on iron via $\rho = \min(\mu, \mu_{Fe})$, where $\mu_{Fe} = \mu^*[dFe]/(K_{Fe} + [sFe])$ has the standard Michaelis-Menten dependency on iron availability, multiplied by the maximum growth rate μ^*. sFe refers to truly dissolved iron (FeL, Fe(II)′, Fe(III)′).

References

Baker, A., Jickells, T., Witt, M., and Linge, K.: Trends in the solubility of iron, aluminium, manganese and phosphorus in aerosol collected over the Atlantic Ocean, Marine Chemistry, 98, 43–58, 2006. 843

Barbeau, K. and Moffett, J.: Dissolution of iron oxides by phagotrophic protists: Using a novel method to quantify reaction rates, Environ. Sci. Technol., 32, 2969–2975, 1998. 827

Barbeau, K., Rue, E., Trick, C., Bruland, K., and Butler, A.: Photochemical reactivity of siderophores produced by marine heterotrophic bacteria and cyanobacteria based on characteristic Fe(III) binding groups, Limnol. Oceanogr., 48, 1069–1078, 2003. 824

Baskaran, M., Santschi, P., Benoit, G., and Honeyman, B.: Scavenging of thorium isotopes by colloids in seawater of the Gulf of Mexico, Geochimica et Cosmochimica Acta, 56, 3375–3388, 1992. 835

Bergquist, B. and Boyle, E.: Dissolved iron in the tropical and subtropical Atlantic Ocean, Global Biogeochem. Cycles, 20, doi:10.1029/2005GB002505, 2006. 832, 844
Brock: Calculating solar radiation for ecological studies, Ecological Modelling, 14, 1–19, 1981. 829
Bruggeman, J., Burchard, H., Kooi, B., and Sommeijer, B.: A second-order, unconditionally stable, mass-conserving integration scheme for biochemical systems, Appl. Num. Math, 57, 36–58, 2006. 829
Burchard, H., Deleersnijder, E., and Meister, A.: Application of Modified Patankar schemes to stiff biogeochemical models for the water column, Ocean Dynamics, 55, 326–337, 2005. 829
Burchard, H., Bolding, K., Kuehn, W., Meister, A., Neumann, T., and Umlauf, L.: Description of a flexible and extendable physical-biogeochemical model system for the water column, J. Mar. Syst., 61, 180–211, 2006. 828
Carlson, C., H.W.Ducklow, and A.F.Michaels: Annual flux of dissolved organic-carbon from the euphotic zone in the northwestern Sargasso Sea, Nature, 371, 405–408, 1994. 831
Cheng, Y., Canuto, V. M., and Howard, A. M.: An improved model for the turbulent PBL, J. Atmos. Sci., 59, 1550–1565, 2002. 828
Cullen, J., Berquist, B., and Moffett, J.: Thermodynamic characterization of partitioning of iron between soluble and colloidal species in the Atlantic Ocean, Mar. Chem., 98, 295–303, 2006. 827, 836
Doney, S., Najjar, R., and Stewart, S.: Photochemistry, mixing and diurnal cycles in the upper ocean, J. Mar. Res., 53, 341–369, 1995. 838
Duce, R. and Tindale, N.: Atmospheric transport of iron and its deposition in the ocean, Limnol. Oceanogr., 36, 1715–1726, 1991. 843
Dutkiewicz, S., Follows, M. J., and Parekh, P.: Interactions of the iron and phosphorus cycles: A three-dimensional model study, Global Biogeochem. Cycles, 19, 1–22, 2005. 825
Emmenegger, L., Schönberger, R., Sigg, L., and Sulzberger, B.: Light-induced redox cycling of iron in circumneutral lakes, Limnol. Oceanogr., 46, 49–61, 2001. 824
Fung, I., Meyn, S., Tegen, I., Doney, S., John, J., and Bishop, J.: Iron supply and demand in the upper ocean, Global Biogeochem. Cycles, 14, 281–301, 2000. 828
Gledhill, M. and van den Berg, C.: Determination of complexation of iron(III) with natural organic complexing ligands in seawater using cathodic stripping voltammetry, Mar. Chem., 47, 41–54, 1994. 824, 836
Jerlov, N.: Optical oceanography, Elsevier, 1968. 829

Jickells, T. and Spokes, L.: Atmospheric iron inputs to the oceans, in: The Biogeochemistry of Iron in Seawater, edited by Turner, D. and Hunter, K., SCOR/IUPAC Series, pp. 85–121, J. Wiley, 2001. 843

Johnson, K., Coale, K., Elrod, V., and Tindale, N.: Iron photochemistry in seawater from the equatorial Pacific, Mar. Chem., 46, 319–334, 1994. 824, 827, 828, 835

Johnson, K., Gordon, R., and Coale, K.: What controls dissolved iron concentrations in the world ocean?, Mar. Chem., 57, 137–161, 1997. 824, 832

King, D., Aldrich, R., and Charniecki, S.: Photochemical redox cycling of iron in NaCl solutions, Mar. Chem., 44, 105–120, 1993. 828

Kuma, K., Nakabayashi, S., Suzuki, Y., Kudo, I., and Matsunaga, K.: Photo-reduction of Fe(III) by dissolved organic substances and existence of Fe(II) in seawater during spring blooms, Mar. Chem., 37, 15–27, 1992. 829

Mahowald, N., Kohfeld, K., Hansson, M., Balkanski, Y., Harrison, S., Prentice, I., Schulz, M., and Rodhe, H.: Dust sources and deposition during the last glacial maximum and current climate: A comparison of model results with paleodata from ice cores and marine sediments, J. Geophys. Res. D. Atmos., 104, 15 895–15 916, 1999. 828

Mahowald, N., Luo, C., Del Corral, J., and Zender, C.: Interannual variability in atmospheric mineral aerosols from a 22-year model simulation and observational data, J. Geophys. Res. D. Atmos., 108, 2003. 825

McClain, C. and Firestone, J.: An investigation of Ekman upwelling in the North Atlantic, J. Geophys. Res., 98, 12 327–12 339, 1993. 832

Moffet, J.: Transformations among different forms of iron in the ocean, in: The Biogeochemistry of Iron in Seawater, edited by Turner, D. and Hunter, K., SCOR/IUPAC Series, pp. 1–7, J. Wiley, 2001. 828, 846, 847

Moran, S. B. and Buesseler, K. O.: Short residence time of colloids in the upper ocean off Bermuda, Nature, 359, 221–223, 1992. 835

Musgrave, D., Chow, J., and Jenkins, W.: Application of a model of upper-ocean physics for studying seasonal cycles of oxygen, J. Geophys. Res., 93, 15 679–15 700, 1988. 832

Nishioka, J., Takeda, S., de Baar, H. J., Croot, P. L., Boye, M., Laan, P., and Timmermans, K. R.: Changes in the concentration of iron in different size fractions during an iron enrichment experiment in the open Southern Ocean, Mar. Chem., 95, 51–63, 2005. 833, 847, 850

Obernosterer, I., Ruardij, P., and Herndl, G.: Spatial and diurnal dynamics of dissolved organic matter (DOM) fluorescence and H_2O_2 and the photochemical demand of surface water DOM

across the subtropical Atlantic Ocean, Limnol. Oceanogr., 46, 632–643, 2001. 837
Ono, S., Najjar, R. G., and Bates, N.: Shallow remineralization in the Sargasso Sea estimated from seasonal variations in oxygen, dissolved inorganic carbon and nitrate, Deep-Sea Res. Part II, 48, 1567–1582, 2001. 832
Oschlies, A. and Schartau, M.: Basin-scale performance of a locally optimized marine ecosystem model, J. Mar. Res., 63, 335–358, 2005. 828, 830, 851
Parekh, P., Follows, M., and Boyle, E.: Modelling the global ocean iron cycle, Global Biogeochem. Cycles, 18(1), GB1002, doi:1029/2003GB002061, 2004. 825, 847, 848
Paulson, C. A. and Simpson, J. J.: Irradiance measurements in the upper ocean, J. Phys. Oceanogr., 7, 952–956, 1977. 829
Rijkenberg, M., Fischer, A., Kroon, J., Gerringa, L., Timmermans, K., Wolterbeek, H., and de Baar, H.: The influence of UV irradiation on the photoreduction of iron in the Southern Ocean, Mar. Chem., 93, 119–129, 2005. 829, 847
Rijkenberg, M. J. A., Gerringa, L. J. A., Neale, P. J., Timmermans, K. R., Buma, A. G. J., and Baar, H. J. W. d.: UVA variability overrules UVB ozone depletion effects on the photoreduction of iron in the Southern Ocean, Geophys. Res. Lett., 31, 1–5, 2004. 824
Rose, A. and Waite, T.: Predicting iron speciation in coastal waters from the kinetics of sunlight-mediated iron redox cycling, Aquatic Sciences, 65, 375–383, 2003. 825
Rue, E. and Bruland, K.: Complexation of iron(III) by natural organic ligands in the Central North Pacific as determined by a new competitive ligand equilibration / adsorptive cathodic stripping voltammetric method, Mar. Chem., 50, 117–138, 1995. 824, 827
Sedwick, P., Church, T., Bowie, A., Marsay, C., Ussher, S., Achilles, K., Lethaby, P., Johnson, R., Sarin, M., and McGillicuddy, D.: Iron in the Sargasso Sea (BATS region) during summer: Eolian imprint, spatiotemporal variability, and ecological implications, Global Biogeochem. Cycles, 19(4), GB4006, doi:10.1029/2004GB002445, 2005. 826, 832, 839, 844, 848, 850, 867
Smith, R. and Baker, K.: Penetration of UV-B and biologically effective dose-rates in natural waters, Photochemistry and Photobiology, 29, 311–323, 1979. 847
Spokes, L. and Jickells, T.: Factors controlling the solubility of aerosol trace metals in the atmosphere and on mixing into seawater, Aquatic Geochemistry, 1, 355–374, 1996. 843
Steinberg, D., Carlson, C., Bates, N., and Johnson, R.J.and Michaels, A. A. K.: Overview of the US JGOFS Bermuda Atlantic Time-series Study (BATS): A decade-scale look at ocean biology and biogeochemistry, Deep-Sea Res. Part II, 48, 1405–1447, 2001. 830

Sunda, W. and Huntsman, S.: Iron uptake and growth limitation in oceanic and coastal phytoplankton, Marine Chemistry, 50, 189–206, 1995. 844, 850
Umlauf, L. and Burchard, H.: Second-order turbulence models for geophysical boundary layers. A review of recent work, Cont. Shelf Res., 25, 795–827, 2005. 828
Uppala, S., Kallberg, P., Simmons, A., Andrae, U., da Costa Bechtold, V., Fiorino, M., Gibson, J., Haseler, J., Hernandez, A., Kelly, G., Li, X., Onogi, K., Saarinen, S., Sokka, N., Allan, R., Andersson, E., Arpe, K., Balmaseda, M., Beljaars, A., van de Berg, L., Bidlot, J., Bormann, N., Caires, S., Chevallier, F., Dethof, A., Dragosavac, M., Fisher, M., Fuentes, M., Hagemann, S., Holm, E., Hoskins, B., Isaksen, L., Janssen, P., Jenne, R., McNally, A., Mahfouf, J.-F., Morcrette, J.-J., Rayner, N., Saunders, R., Simon, P., Sterl, A., Trenberth, K., Untch, A., Vasiljevic, D., Viterbo, P., and Woollen, J.: The ERA-40 re-analysis, Q. J. R. Meteorol. Soc., 131, 2961–3012, 2005. 829
Van den Berg, C.: Evidence for organic complexation of iron in seawater, Mar. Chem., 50, 139–157, 1995. 824, 827, 836
Voelker, B. and Sedlak, D.: Iron reduction by photoproduced superoxide in seawater, Mar. Chem., 50, 93–102, 1995. 837
Voelker, B. and Sulzberger, B.: Effects of fulvic acid on Fe(II) oxidation by hydrogen peroxide, Environmental Science & Technology, 30, 1106–1114, 1996. 824
Waite, T. and Morel, F.: Photoreductive dissolution of colloidal iron oxides in natural waters, Environ. Sci. Technol., 18, 860–868, 1984. 827
Watson, A.: Iron limitation in the ocean, in: The Biogeochemistry of Iron in Seawater, edited by Turner, D. and Hunter, K., SCOR/IUPAC Series, pp. 9–39, J. Wiley, Chichester, 2001. 828
Weber, L., Völker, C., Schartau, M., and Wolf-Gladrow, D.: Modeling the speciation and biogeochemistry of iron an the Bermuda Atlantic Timeseries Study site, Global Biogeochem. Cycles, 19(1), GB1019, doi:10.1029/2004GB002340, 2005. 825, 826, 827, 828, 831, 832, 834, 835, 836, 837, 842, 844, 848, 849, 851, 859, 861
Wells, M.: Marine Colloids and Trace Metals, in: Marine Dissolved Organic Matter, edited by Hansell, D.A. and C.A. Carlson, pp. 367–404, Academic Press, Elsevier, 2002. 835
Wells, M. and Mayer, L.: The photoconversion of colloidal iron oxyhydroxides in seawater, Deep-Sea-Res., 38, 1379–1395, 1991. 827
Wen, L.-S., Santschi, P., and Tang, D.: Interactions between radioactively labeled colloids and natural particles: Evidence for colloidal pumping, Geochimica et Cosmochimica Acta, 61, 2867–2878, 1997. 824, 835, 850

Witter, A. and Luther III, G.: Variation in Fe-organic complexation with depth in the northwestern Atlantic Ocean as determined using a kinetic approach, Mar. Chem., 62, 241–258, 1998. 824, 827

Witter, A., Hutchins, D., Butler, A., and Luther III, G.: Determination of conditional stability constants and kinetic constants for strong model Fe-binding ligands in seawater, Mar. Chem., 69, 1–17, 2000. 824

Wu, J. and Boyle, E.: Determination of iron in seawater by high-resolution isotope dilution inductively coupled plasma mass spectrometry after $Mg(OH)_2$ coprecipitation, Analytica Chimica Acta, 367, 183–191, 1998. 826, 839, 867

Wu, J. and Boyle, E.: Iron in the Sargasso Sea: Implications for the processes controlling dissolved Fe distribution in the ocean, Global Biogeochem. Cycles, 16(4), 1086, doi:10.1029/2001GB001453, 2002. 826, 832, 839

Wu, J. and Luther III, G.: Size-fractionated iron concentrations in the water column of the western North Atlantic Ocean, Limnol. Oceanogr., 39, 1119–1129, 1994. 826, 839, 867

Wu, J. and Luther III, G.: Complexation of Fe(III) by natural organic ligands in the Northwest Atlantic Ocean by a competitive ligand equilibration method and a kinetic approach, Mar. Chem., 50, 159–177, 1995. 824, 827, 836

Wu, J., Boyle, E., Sunda, W., and Wen, L.-S.: Soluble and colloidal iron in the oligotrophic North Atlantic and North Pacific, Science, 293, 847–849, 2001. 826, 848

Zhuang, G., Duce, R., and Kester, D.: The dissolution of atmospheric iron in the surface seawater of the open ocean, J. Geophys. Res., 95, 16 207–16 216, 1990. 843

Table 1. Parameters of the NPZD Model.

Parameter	Symbol	Unit	Value
	Biology		
maximum growth rate	μ^*	d^{-1}	0.27
phytoplankton mortality	γ_p	d^{-1}	0.04
initial slope P-I curve	α	$m^2\ W^{-1}\ d^{-1}$	0.256
nitrate half-saturation constant	K_N	μM	0.7
iron half-saturation constant	K_{Fe}	nM	0.2
phytoplankton aggregation rate	γ_{p^2}	$\mu M^{-1}\ d^{-1}$	0.025
maximum grazing rate	g	d^{-1}	1.575
prey capture rate	ϵ	$\mu M^{-1}\ d^{-1}$	1.6
assimilation efficiency	γ_{za}	-	0.925
excretion	γ_{zb}	d^{-1}	0.01
quadratic mortality	γ_{z^2}	$\mu M^{-1}\ d^{-1}$	0.34
detritus remineralisation	γ_d	d^{-1}	0.048
sinking velocity	w_s	$m\ d^{-1}$	18
coefficient for temperature function	C_{ref}	-	1.066
PAR:short-wave irradiance ratio	f_{PAR}	-	0.43
attenuation due to chlorophyll	κ	$(mg\ Chl)^{-1}\ L\ m^{-1}$	0.03
maximum Fe:N ratio in organic matter	$r_{Fe:N}$	$nM\ \mu M^{-1}$	$3.31 \cdot 10^{-2}$
mass:N ratio in organic matter	$r_{m:N}$	$g\ mol^{-1}$	159

Table 2. Parameters of the chemical model from the zero-dimensional model by Weber et al. (2005) (Run I) and changed parameters in the one-dimensional model of the present study (Run A).

Parameter	Symbol	Unit	Run I	Run A
Chemistry				
Fe(II)′ oxidation rate by O_2	k_{ox1}	$\mu M^{-1}\ d^{-1}$	0.864	–
oxygen concentration	$[O_2]$	μM	214	–
Fe(II)′ oxidation rate by O_2^-	k_{ox2}	$nM^{-1}\ d^{-1}$	864	–
Fe(II)′ oxidation rate by H_2O_2	k_{ox3}	$nM^{-1}\ d^{-1}$	6.24	–
Fe_{col} photoreduction rate at 30 μE $m^{-3}\ s^{-1}$	k_{ph1}	d^{-1}	20.16	1.32
FeL photoreduction rate at 30 μE $m^{-3}\ s^{-1}$	k_{ph2}	d^{-1}	86.4	–
Fe(III)′ photoreduction rate at 30 μE $m^{-3}\ s^{-1}$	k_{ph3}	d^{-1}	1.32	–
Fe_p photoreduction rate at 30 μE $m^{-3}\ s^{-1}$	k_{ph4}	d^{-1}	20.2	–
Fe_{col} formation rate	k_{col}	d^{-1}	2.4	-
FeL formation rate	k_{fel}	$nM^{-1}\ d^{-1}$	172.8	-
FeL conditional stability constant	k_{ld}	M^{-1}	$10^{20.3}$	10^{22}
free organic ligand concentration	$[Lig]$	nM	–	2.4
Fe(III)′ reduction rate by O_2^-	k_{red}	$nM^{-1}\ d^{-1}$	$1.3 \cdot 10^4$	–
Fe(III)′ scavenging rate	k_{sca}	$kg^{-1}\ l\ d^{-1}$	$2.5 \cdot 10^4$	–
Fe_{col} aggregation rate	k_{ag}	$kg^{-1}\ l\ d^{-1}$	$1.224 \cdot 10^6$	–
O_2^- dismutation rate	k_{dm}	$nM^{-1}\ d^{-1}$	2.64	-
O_2^- production rate at 30 μE $m^{-3}\ s^{-1}$	$S_{O_2^-}$	$nM\ d^{-1}$	1037	–
H_2O_2 decay rate	k_{dis}	d^{-1}	0.24	–
solubility of atmospheric iron	k_{sol}	%	1	–
Total Cu concentration	$[Cu_T]$	nM	1	–
Cu(I) oxidation rate by O_2^-	k_{cuox}	$nM^{-1}\ d^{-1}$	$8.1 \cdot 10^5$	–
Cu(II) reduction rate by O_2^-	k_{cured}	$nM^{-1}\ d^{-1}$	$1.4 \cdot 10^3$	–

Table 3. Maximum redox rates in nM d^{-1} at noon in August.

Rate	1 m depth	40 m depth	100 m depth
k_{ox1}	70.52	10.84	0.40
k_{ox2}	424.10	14.84	0.05
k_{ox3}	454.10	21.44	0.06
k_{red}	871.80	41.37	0.24
k_{ph1}	0.44	0.04	0.00
k_{ph2}	40.37	5.51	0.34
k_{ph3}	0.19	0.00	0.00
k_{ph4}	0.01	0.00	0.00

Table 4. Change in modeled dFe concentration [%] of the parameter sensitivity study with the one-dimensional model of the present study (1-D) and the zero-dimensional model by Weber et al. (2005) (0D). Zero values correspond to changes smaller than 0.5%. Surf = upper 100 m.

	Surf Mean		Surf Max		Surf Min		250 Mean	
Parameter	double	half	double	half	double	half	double	half
1D								
k_{sol}	**13**	**–6**	**36**	**–18**	**10**	**–6**	3	–2
$r_{Fe:N}$	**–7**	3	**–7**	4	**–9**	**5**	2	–1
k_{ag}	**–5**	2	**–5**	3	**–7**	4	**–7**	4
k_{col}	–1	1	–1	1	–2	2	–2	2
k_{fel}	1	–1	1	0	1	–1	0	–1
k_{ld}	1	–1	1	–1	1	–2	1	–2
k_{sca}	0	0	0	0	0	0	0	0
k_{ox1}	0	0	0	0	0	0	0	0
k_{ox2}	0	0	0	0	0	0	0	0
k_{ox3}	0	0	0	0	0	0	0	0
k_{ph1}	1	–1	1	0	1	–1	0	0
k_{ph2}	1	–1	0	–1	1	–1	0	0
k_{ph3}	0	0	0	0	0	0	0	0
k_{ph4}	0	0	0	–1	1	–1	0	0
k_{red}	0	0	0	0	0	0	0	0
0D								
k_{sol}	2	–1	**7**	–3	1	0	–	–
$r_{Fe:N}$	–2	1	–1	0	**–8**	4	–	–
k_{ag}	–3	2	0	0	**–17**	**11**	–	–
k_{col}	–1	1	0	0	–4	5	–	–
k_{fel}	0	0	0	0	1	–3	–	–
k_{ld}	0	0	0	0	0	0	–	–
k_{sca}	0	0	0	0	0	0	–	–
k_{ox1}	0	0	0	0	0	0	–	–
k_{ox2}	0	0	0	0	0	0	–	–
k_{ox3}	0	0	0	0	0	0	–	–
k_{ph1}	1	–1	0	0	5	–4	-	–
k_{ph2}	0	0	0	0	0	0	–	–
k_{ph3}	0	0	0	0	0	0	–	–
k_{ph4}	1	–1	0	0	**8**	**–8**	–	–
k_{red}	0	0	0	0	0	0	–	–

Table 5. Annually concentration of dFe [nM] of model runs with varying redissolution processes. surf= upper 100 m, 0.000 = values smaller than 0.001.

		dFe			
Run	Parameter	surf mean	surf max	surf min	250 m mean
I	initial	0.015	0.198	0.000	0.000
A	standard	0.610	0.852	0.562	0.582
r1	with k_{pd}	0.161	0.833	0.027	0.050
r2	with k_{cd}	0.185	0.911	0.015	0.001
r3	with k_{pd} and k_{cd}	0.263	0.962	0.087	0.122

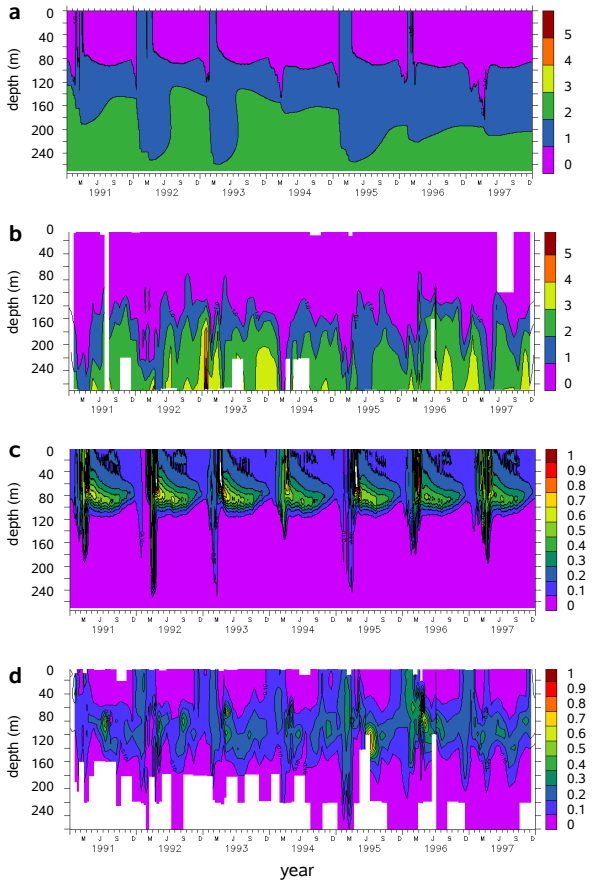

Fig. 1. Modeled (a+c) and observed (b+d) concentrations of DIN (Nitrate + Nitrite) in μM (a+b) and chlorophyll α in μg l^{-}1 (c+d). Observed values were taken from BATS bottle observations and linearly interpolated in the vertical.

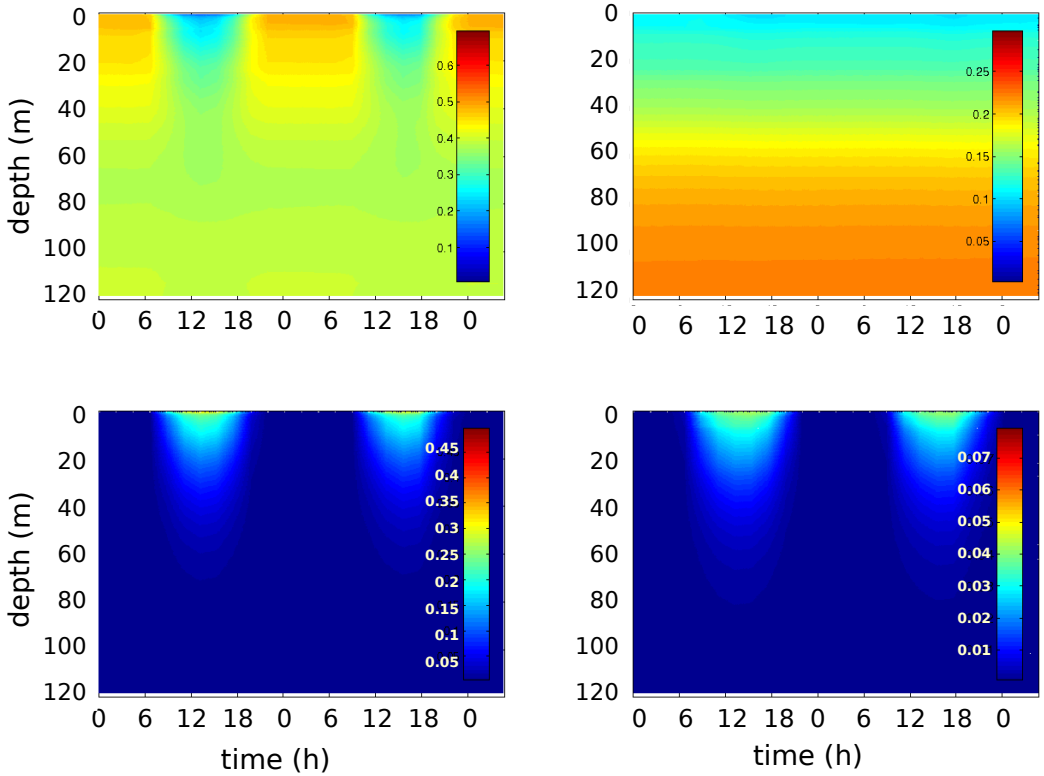

Fig. 2. Diurnal variability of modeled iron concentrations in nM for a typical summer day (2 August 1994). The figures show FeL (top left), Fe_{col} (top right), $Fe(II)'$ (bottom left) and $Fe(III)'$ (bottom right).

BGD
4, 823–869, 2007

EGU

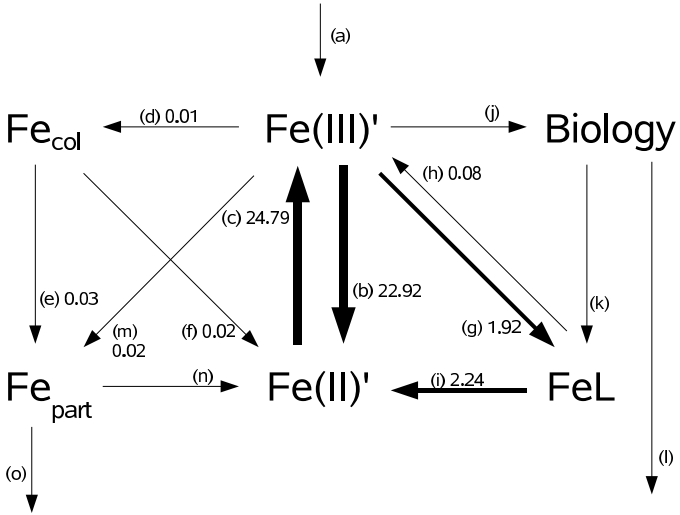

Fig. 3. Schematic representation of the iron pools represented in the model and the fluxes between them and their annually averaged rates of change of modeled iron concentrations [nM d^{-1}] in 0–40 m depth. Arrows without number are smaller than 0.01. The fluxes are not balanced because of the missing vertical fluxes in this figure. (a) dust deposition, (b) reduction by light and O_2^-, (c) oxidation by O_2, O_2^- and H_2O_2, (d) formation of colloids, (e) aggregation, (f) photoreduction, (g) FeL formation, (h) FeL dissociation, (i) photoreduction, (j) biological uptake, (k) remineralisation, (l) sinking, (m) adsorption, (n) photoreduction, (o) sinking.

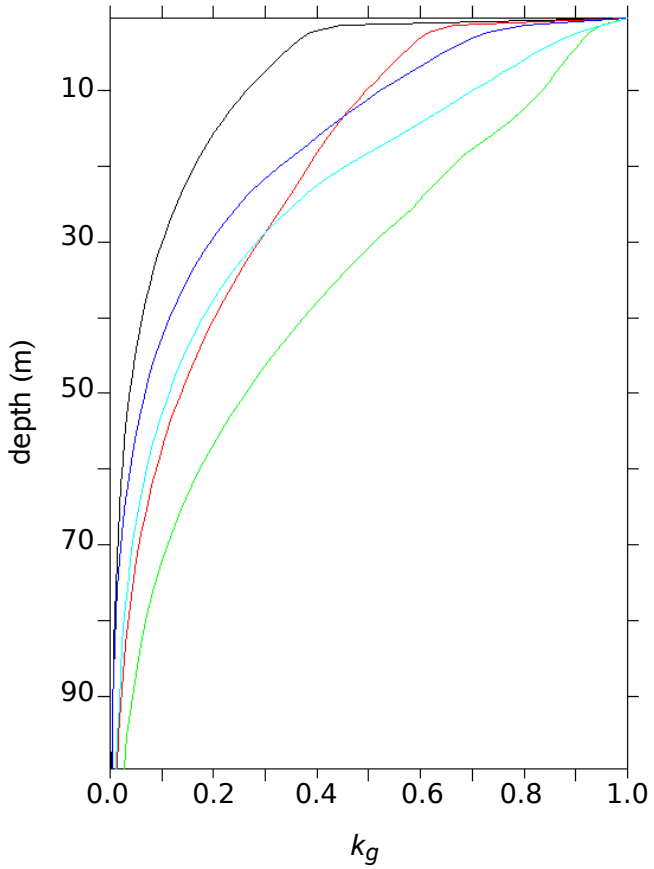

Fig. 4. Concentration difference (noon minus midnight) for several phochemically influenced species (red: O2-, blue: Fe(II)′, magenta: Fe(III)′, green: H_2O_2) and downwelling irradiation (black) as a function of depth. All concentration differences have been scaled to one at the surface to make the different vertical scales visible. Average for the period 1 June–31 August.

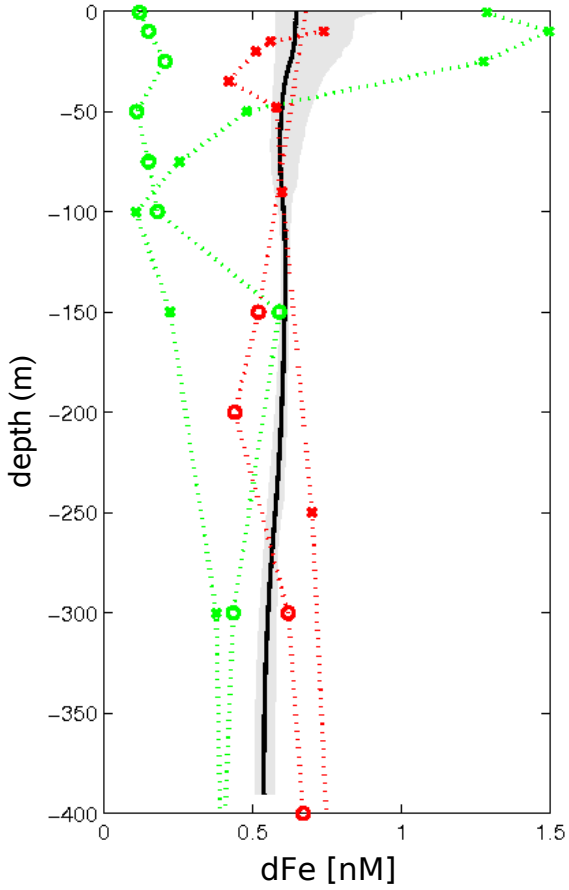

Fig. 5. Annual mean profile of modeled dFe concentration (black line) with maximum (summer) and minimum (spring) values (area in light gray). Measured dFe concentration at BATS in spring (circle) and summer (cross) by Wu and Luther III (1994); Wu and Boyle (1998) (red) and Sedwick et al. (2005) (green).

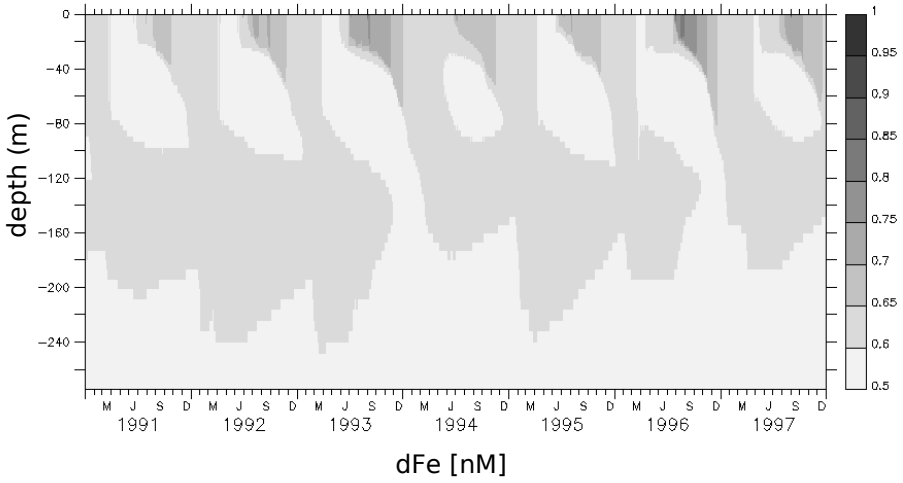

Fig. 6. Modeled concentrations of dFe in nM (Model Run A).

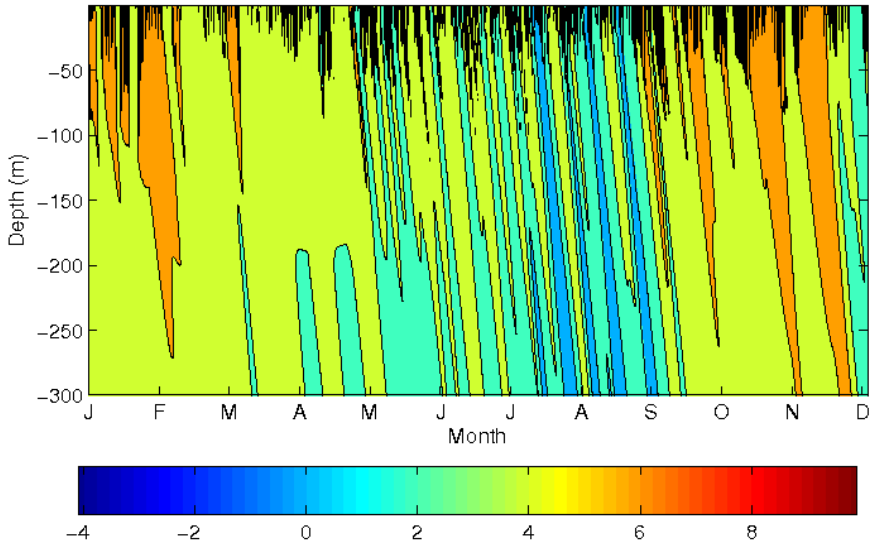

Fig. 7. Residence-time of dFe in years (log-scale) in the upper 40 m.